Available online at www.sciencedirect.com
SCIENCE DIRECT®
ELSEVIER
Ultramicroscopy 97 (2003) 451–458
ultramicroscopy
www.elsevier.com/locate/ultramic

IR imaging using uncooled microcantilever detectors

L.R. Senesac[a], J.L. Corbeil[a,b], S. Rajic[a,b], N.V. Lavrik[a], P.G. Datskos[a,b,*]

[a] *Oak Ridge National Laboratory, P.O. Box 2008, Oak Ridge, TN 37831-6141, USA*
[b] *University of Tennessee, 401 Nielsen Physics Bldg., Knoxville, TN 37996-1200, USA*

Received 15 July 2002; received in revised form 14 October 2002

Abstract

Uncooled bimaterial microcantilever detectors were fabricated and used to obtain infrared (IR) images of objects at temperatures ranging from room temperature to a few hundred °C. Images were obtained using both single 50 μm × 50 μm microcantilever IR detectors and arrays of microcantilever detectors. Thermal radiation from the target object was imaged onto the detector and the resulting temperature change caused microcantilever bending due to the bimaterial effect. This micromechanical bending was measured using two different non-contact optical readout techniques and IR images were obtained. A smaller size (20 μm × 20 μm) microcantilever IR detector was also used to capture IR images of near room temperature objects.
© 2003 Elsevier Science B.V. All rights reserved.

Keywords: IR imaging; Microcantilever; IR sensors; IR detectors

1. Introduction

The detection and imaging of thermal infrared (IR) radiation has many commercial, industrial, medical, and military applications [1–3]. Limiting factors to present day IR imaging have been the high cost of IR cameras and the high power consumption required for detector cooling and readout electronics [4–11]. Our present work is aimed to overcome these limitations by developing simple, low cost uncooled microcantilever detector arrays with a low power non-contact optical readout [12, 13]. The microcantilever detector arrays we developed for uncooled IR imaging can be fabricated using standard semiconductor processing technology and require no electrical connections or onboard electronics.

The individual microcantilever detectors in an imaging array bend in response to incident IR radiation due to the bimaterial effect [13–17]. As the temperature of the bimaterial structure changes, the lengths of the two layers change by different amounts and the resulting stress causes the structure to bend [18]. Earlier work has shown that microcantilever bending can readily be determined by a number of means, including optical, capacitive, piezoresistive, and electron tunneling with extremely high sensitivity [19–21]. For example, the metal-coated microcantilevers that are commonly employed in atomic force microscopy (AFM) allow sub-Angstrom

*Corresponding author. Oak Ridge National Laboratory, 1 Bear Creek Road, Oak Ridge, TN 37831-8039, USA. Tel.: +1-865-574-6205; fax: +1-865-574-9704.
E-mail address: pgd@ornl.gov (P.G. Datskos).

0304-3991/03/$ - see front matter © 2003 Elsevier Science B.V. All rights reserved.
doi:10.1016/S0304-3991(03)00073-1

($<10^{-10}$ m) sensitivity to be routinely obtained [20, 21].

In our present work, the microcantilever bending due to IR absorption is observed by a non-contact optical readout technique. For our experiments, two different non-contact readout techniques were employed. One technique, termed the "quad-cell readout", uses an approach similar to that used in conventional AFM and is useful for measuring the bending of single detectors. The second technique, termed the "CCD readout", uses a read laser and charged coupled device (CCD) camera (or a CMOS camera) to record images either of a single IR detector or of an array of IR detectors. Processing of the images captured by the CCD camera allows us to determine the bending of individual microcantilever.

2. Fabrication

During the initial steps in our design and investigation of microcantilever IR detectors, a single element detector is easier to fabricate, modify, and test. For this reason, single cantilever detectors of a particular geometry and material combination are first fabricated and investigated to determine the performance characteristics and optimize their response. In this manner designs which yield the best performance are then selected to be used in focal plane array fabrication.

2.1. Fabrication of single detectors with focused ion beam milling

The fabrication of the single microcantilever detector is performed using a focused ion beam (FIB) milling system (FEI 200) [22–24]. The device shown in Fig. 1 was fabricated using our FIB system. The device is composed of an IR radiation absorbing area and two legs which provide mechanical support, thermal isolation, and bimaterial bending. The material used was a 0.6 μm thick sheet of SiN_x with a 50 nm coating of Al. The FIB was used to direct write the pattern of the device by rastering the ion beam over a user-defined area. The large center portion of the detector is the IR radiation absorption area with dimensions of 36 μm × 50 μm. The incident IR radiation is absorbed by the SiN_x layer and when the device is placed in an evacuated chamber the principal mechanism loss of heat dissipation occurs through the legs attached to the substrate. The leg cross section is 2 μm (wide) × 0.6 μm (thick). The Al was removed from the center leg section to increase the thermal isolation while maintaining the bimaterial effect from the outer support legs. This isolation area increases the time required for the heat to escape from the IR absorbing area and thereby increases the temperature gradient across the bimaterial portion of the leg. This increased temperature gradient enhances the bimaterial bending and thus increases the response of the detector. When taking into account both the absorption area and support leg area, the overall device is equivalent to a 50 μm × 50 μm IR detector.

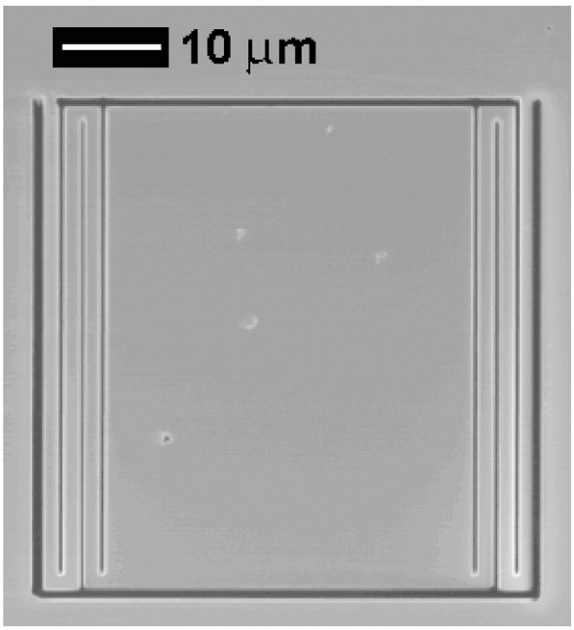

Fig. 1. FIB image of a 50 μm × 50 μm microcantilever detector.

2.2. Fabrication of arrays of detectors

The diagram in Fig. 2 illustrates the basic steps used for array fabrication. The process combines several techniques, all of which are standard processes in the semiconductor microfabrication

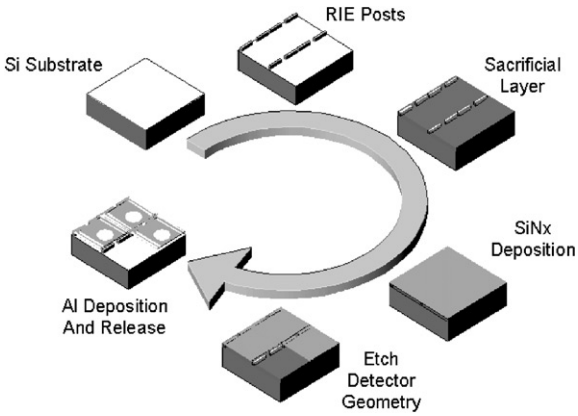

Fig. 2. Microfabrication process diagram for the production of arrays of microcantilever detectors.

industry. The initial material was a Si substrate and reactive ion etching was used to remove portions of the Si to create the posts necessary for anchoring the detectors. The posts were 3.5 μm tall. Next a layer of sacrificial material was deposited and the surface was chemomechanically polished (CMP) until the layer and posts were 2.5 μm high, leaving the surface flush with the tops of the posts. SiN_x was the principle material of the detector and was deposited as a uniform 300 nm thick layer directly on top of the posts and sacrificial layer. The sacrificial layer was required to provide a uniform 2.5 μm spacing between the substrate and the SiN_x layer which served as an IR resonant cavity.

The next step involved reactive ion etching which was used to define the detector geometry into the SiN_x layer. A 120 nm layer of Al was deposited and patterned through a photolithographic mask to form the bimaterial leg sections and a reflective surface on the head of the detector for use by the readout laser. Finally, the sacrificial layer was chemically removed leaving an array of released detectors.

In Fig. 3, a portion of a 256×256 array of microcantilever IR detectors is shown. The detectors are placed with a 50 μm square pitch. Also shown is a close-up of one of the detectors in which the patterning of the deposited Al layer is readily apparent. The lighter color on the detector head is the bare SiN_x, and the darker color area on the detector head indicate the presence of Al. The

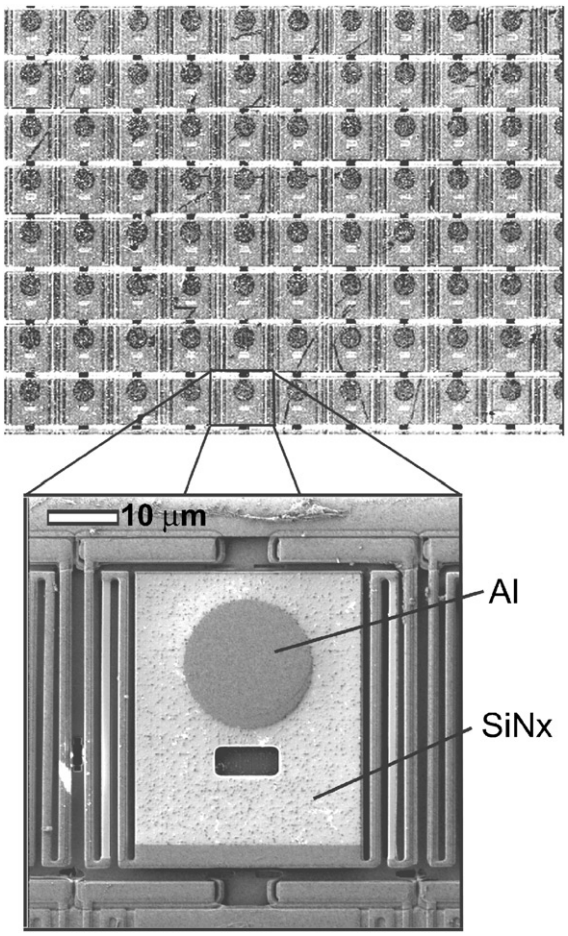

Fig. 3. FIB image of a portion of a 256×256 detector array (top) and a close-up image (bottom) of an individual detector.

dark color circle served as a reflective area for the optical readout. The small rectangular opening just below the center of the detector is an etch release hole needed to allow etching chemicals to remove the sacrificial layer under the detector.

3. Experimental

The readout of the microcantilevers used in the present work was performed using two different optical readout schemes. In each case the image of an IR target was formed at the position of the microcantilever detector by an IR lens. As the microcantilever detector absorbs the IR radiation

and increases its temperature a bending occurs due to the bimaterial layer [15, 25–27]. This bending is then measured and analyzed to determine the response of the detector. The main difference between the two readout schemes lies in the specific manner in which the actual bending of the microcantilever is detected and measured.

3.1. Quad-cell readout

The basic components of the quad-cell readout are shown in Fig. 4. The IR target was mounted on a computer-controlled motorized stage. The IR radiation from the target passed through a mechanical chopper and was focused onto the microcantilever detector by an IR lens. The mechanical chopper was necessary to provide a reference frequency to a lock-in amplifier used to reject signal noise and increase the measured signal-to-noise ratio. The detector was mounted in a vacuum cell to prevent detector heat loss due to thermal convection, thus increasing the detectors thermal isolation. The pressure in the vacuum cell was typically a few mTorr. The vacuum cell had a germanium window to allow incoming IR radiation to fall onto the detector, and a quartz window on the readout side to transmit the visible light from the readout laser.

The bending of the microcantilever detector was measured by a quad-cell optical readout. A laser was focused onto the detector and the reflected spot was incident on a quad-cell position-sensitive detector (PSD). As the microcantilever detector bent in response to the IR radiation, the reflected spot from the microcantilever moved on the quad-cell PSD and a signal voltage was produced which was proportional to the motion of the spot. This signal voltage was monitored by a lock-in amplifier which was phase locked to the reference frequency provided by the mechanical chopper, and output of the lock-in amplifier was recorded by a computer.

For the image scan, the IR target was rastered back and forth by the computer-controlled motorized stage. The signal from the lock-in amplifier was recorded by the computer and the final IR image of the target was constructed by scaling the data into an 8-bit array (256 levels of grayscale), where the minimum microcantilever deflection was displayed as black and the maximum deflection as white.

3.2. CCD readout

The quad-cell readout works very well for single element detectors, but for arrays of thousands or millions of detectors, this method becomes impractical. This was the motivation for developing a CCD readout. The basic components of the CCD readout are shown in Fig. 5. The IR radiation from the target was focused onto the detector as before; however, a collimated readout laser was employed to illuminate the entire array at once. The reflected laser light from the array was observed with a microscope focused on the array surface and this image was captured by a 12-bit CCD camera. In the case of the quad-cell readout the readout laser was focused onto a single detector, concentrating approximately 5 mW of

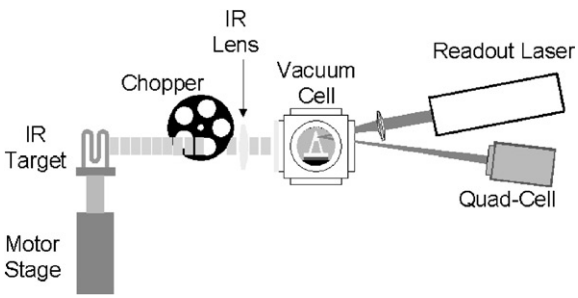

Fig. 4. Diagram of the experimental setup for the quad-cell readout.

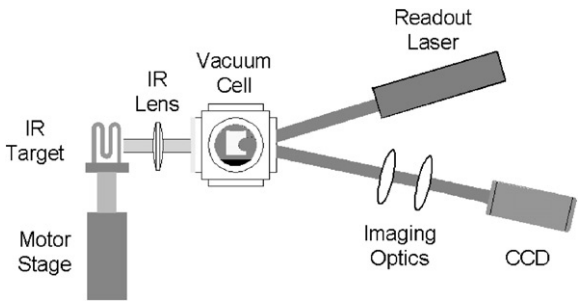

Fig. 5. Diagram of the experimental setup for the CCD readout.

power on the device. For the CCD readout, the same beam was expanded and collimated so that the total power incident on a single detector was on the order of a few nW. The CCD readout requires much less energy per detector for the device readout.

The CCD readout was used to produce IR images with a single IR detector as well as with arrays of detectors. For a single detector the IR target was rastered in an x–y grid and a CCD image of the IR detector was captured at each x–y point. As the cantilever deflected in response to the incident IR radiation the intensity of the reflected light from the readout laser changed, and these changes in intensity were recorded in the captured CCD images. Each image was then analyzed to measure this intensity change and the result was recorded as a final image pixel value. The final image is therefore a point-by-point record of the IR detector deflection as the IR target was rastered in front of the microcantilever IR detector. Again the data was grayscaled for display purposes with the minimum cantilever deflection displayed as black and the maximum deflection as white.

In order to make an IR image of the target using an array of IR detectors, the first step was to capture a background image (a CCD image of the detector array with no IR stimulus). The IR target was then imaged onto the detector by the IR optics and the absorbed IR radiation caused the micro-cantilever detectors to bend. A second CCD image of the detector array was then captured and the background image was subtracted from it. The resulting image is the difference in reflected light intensity from the entire array as it responds to the IR stimulus. This difference image was then analyzed to extract a single number for each IR detector which corresponded to the change in intensity for that detector. These values were then recorded as the pixels of the final IR image.

4. Results and discussion

4.1. IR imaging with single detector

The experimental results for IR imaging with a single detector for both readout schemes may be seen in Fig. 6. The top image is a photo of the IR target. The target was made by bending a wire into the shape of the script logo of our laboratory: Oak Ridge National Laboratory, 'ornl'. The center image in Fig. 6 is the scanned image of the target taken with the quad-cell readout. The temperature of the wire was $\sim 350°C$. The image resolution is 600 points horizontally and 100 points vertically. The grayscale from black to white corresponds to temperature differences from minimum to maximum.

The bottom image in Fig. 6 is the scanned image of the same target taken with the CCD readout. The image resolution is 850 points horizontally and 100 points vertically. The grayscale from black to white corresponds to temperature differences from minimum to maximum.

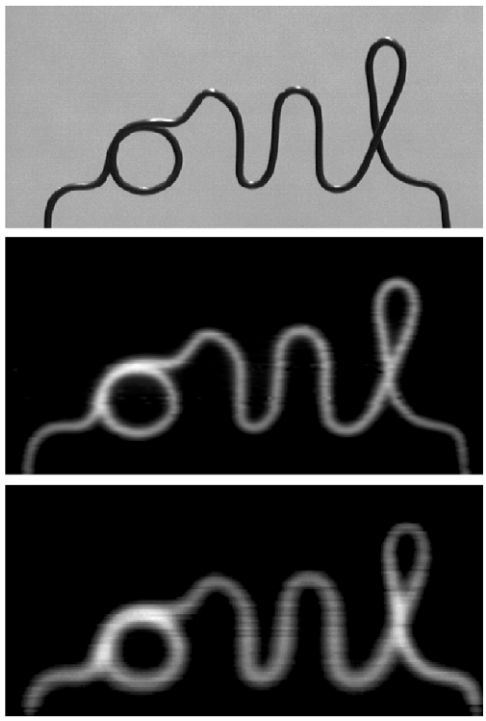

Fig. 6. The top image is a photo of the target object to be imaged. It is a wire bent in the shape of script logo 'ornl' for Oak Ridge National Laboratory. The center image is a scanned image of the target made with the quad-cell readout. The bottom image is a scanned image of the target made with the CCD readout.

4.2. IR imaging with an array of detectors

For the first imaging tests using a detector array, a 44×43 detector section was chosen from a 256×256 array of IR detectors. This imaging array had a uniform coating of Al over the entire surface, and therefore did not have the optimal thermal isolation obtained with the single detectors tested. As a result, the temperature of the targets had to be substantially increased as compared with the single detector tests. The results of the first test can be seen in Fig. 7. The photo on the left shows a commercially available blackbody source used as the IR target. The temperature of the source is 900°C. The image on the lower right of Fig. 7 (directly below the close-up view of the circular source) is the 44×43 pixel image of the target produced with the CCD readout. We should point out that the temperature is imaged as hotter near the center and cools slightly toward the perimeter of the blackbody source.

The second test involved imaging the 'ornl' test wire as in the single pixel tests above. The temperature of the wire was $\sim$700°C. The 44×43 detector array section was used and the results may be seen in Fig. 8. At the top is the photo of the wire shown again here for comparison purposes. The center left image is the 400×400 pixel CCD image of the 44×43 IR detector array after background subtraction. The CCD image contains an approximately 9×9 pixel picture of each detector in the IR detector array. These 81 pieces of data can then be analyzed for intensity changes to produce a single pixel value for the final image. This final 44×43 image is shown at the center right of Fig. 8. At the bottom left of Fig. 8 is a photo of a stove-heating element and at the bottom right is an IR image of the element made with a 64×64 array of detectors. The temperature of the heating element was 190°C.

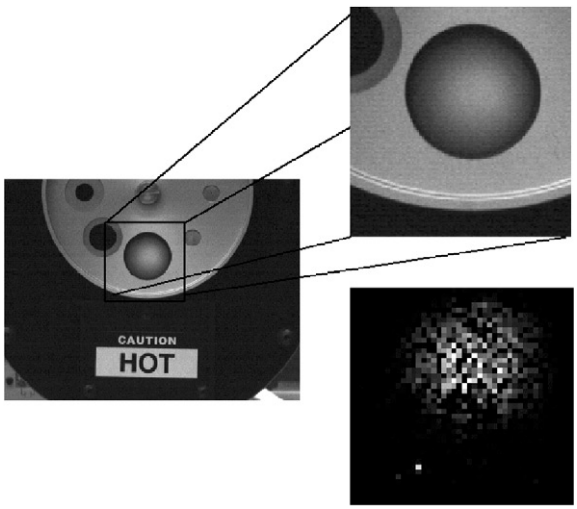

Fig. 7. The images on the left and close-up in the upper right are photos of blackbody source. The image in the lower right is the IR image of the source made with a 44×43 detector array section using the CCD readout.

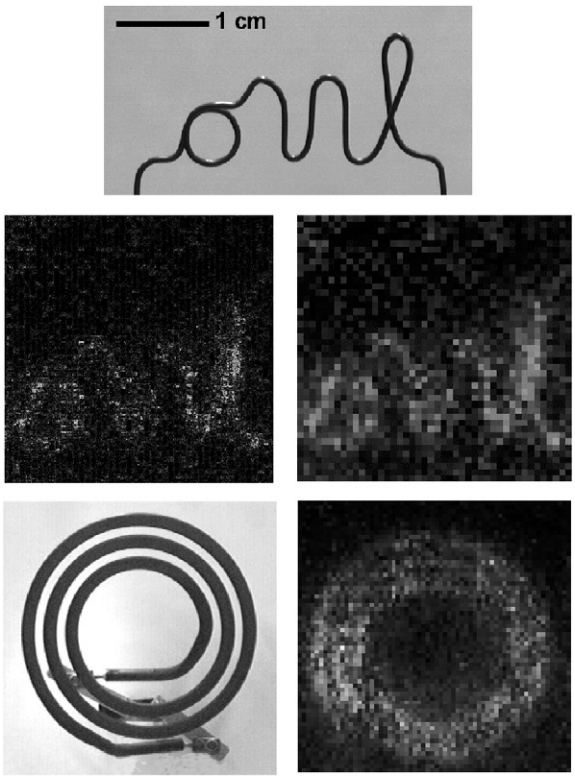

Fig. 8. The upper image is a photo of the 'ornl' wire target. The image on the center left is a 400×400 pixel CCD image of the 44×43 detector array after background subtraction and the final 44×43 pixel IR image is shown at the center right. The image at the bottom left is a photo of the stove heating element and to the immediate right is the final 64×64 IR image of the element.

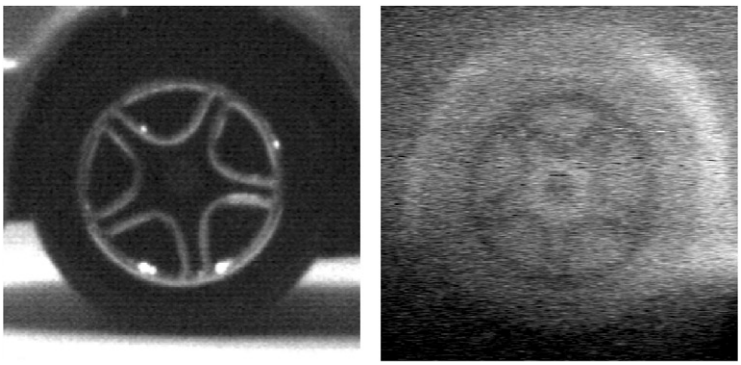

Fig. 9. IR image made with 20 μm × 20 μm detector. The image on the left is the IR target at a temperature of 34°C. On the right is the IR image made using the quad-cell readout.

4.3. IR imaging with a 20 μm × 20 μm detector

As the array was being fabricated, newer pixel geometries were being tested. Detector size is an important parameter due to the fact that image resolution is ultimately determined by the detector density of the array, i.e., for a given format (allowable array size for a specific application) the higher the density of the detectors, the more detectors may be incorporated into the array, giving a higher resolution. The results of preliminary tests of a 20 μm × 20 μm detector are shown in Fig. 9. The image on the left is a photo of the IR target at a temperature of 34°C. The image on the right shows the IR image obtained using the quad-cell readout. The image resolution is 450 points horizontally and 150 points vertically. The design details of this detector are published elsewhere.

5. Conclusions

We obtained IR images of objects using both single uncooled microcantilever IR detectors and arrays of microcantilever detectors. The single detector images appear sharper for the following reasons. First, the necessity of rastering the target to produce the image enables the resolution of the image to be arbitrarily high, i.e. by changing the number and spacing of points in the x–y scan we can make the number of pixels in the final image be as large as desired. The section of the array of detectors used was limited to 44 × 43 detectors for the 'ornl' test wire image and 64 × 64 detectors for the stove heating element image, and therefore the final image resolution was much lower than in the rastered single detector images (∼600 × 100). A second reason for a difference in image quality is due to differences in detector thermal isolation. The single detector had Al removed from a leg section (as described above) to increase the thermal isolation of the detector, while the detector array did not. This is also the reason that the target temperatures were higher for the detector array tests. The fabrication and testing of an array of detectors with this thermal isolation is expected to occur in the near future.

We also obtained an IR image with a new 20 μm × 20 μm detector design which had an optimized isolation section. This detector is smaller than typical IR detectors. Room temperature objects emit IR radiation at a wavelength of about 10 μm, therefore a 20 μm pixel is approaching the diffraction limit for a detector at these wavelengths.

Two different non-contact optical readout schemes were used to produce the images. The quad-cell readout benefits from the use of a mechanical chopper used with a lock-in amplifier to reduce noise in the quad-cell signal. The CCD readout gave comparable results with no mechanical chopper and therefore requires less power and has no moving parts as compared to the quad-cell readout.

Acknowledgements

We like to acknowledge support from the Defense Advanced Research Projects Agency, the National Science Foundation and the US Department of Energy. This work was partially supported by the Laboratory Director's Research and Development Program of Oak Ridge National Laboratory. Oak Ridge National Laboratory is operated for the US Department of Energy by UT-Battelle under contract DE-AC05-96OR22464.

References

[1] J.M. Lloyd, Thermal Imaging Systems, Plenum Press, New York, 1975.
[2] J.L. Miller, Principles of Infrared Technology, Van Nostram Reinhold, New York, 1994.
[3] R.S. Balcerak, Infrared Technol. Appl. XXV, SPIE 3698 (1999) 110.
[4] P.W. Kruse, L.D. McGlauchlin, R.B. McQuistan, in: Elements of Infrared Technology, Wiley, New York, 1962, p. 351.
[5] P.W. Kruse, L.D. McGlauchlin, R.B. McQuistan, Elements of infrared technology, Wiley, New York, 1962.
[6] P.W. Kruse, Infrared Phys. Technol. 34 (1994) 25.
[7] P.W. Kruse, Infrared Technol. XXI, SPIE 2552 (1995) 556.
[8] P.W. Kruse, Infrared Phys. Technol. 36 (1995) 869.
[9] P.W. Kruse, in: P.W. Kruse, D.D. Skatrud (Eds.), Uncooled Infrared Imaging Arrays and Systems, Semiconductors and Semimetals, Vol. 47, Academic Press, San Diego, 1997.
[10] P.W. Kruse, Uncooled Thermal Imaging, Arrays Systems and Applications, SPIE Press, Bellingham, WA, 2001.
[11] A.S. Jensen, Infrared Technol. XIX, SPIE 2020 (1993) 340.
[12] P.G. Datskos, S. Rajic, L.S. Senesac, D.D. Earl, B.M. Evans, J.L. Corbeil, I. Datskou, Infrared Technol. Appl. XXVI, SPIE 4130 (2000) 185.
[13] T. Perazzo, M. Mao, O. Kwon, A. Majumdar, J.B. Varesi, P. Norton, Appl. Phys. Lett. 74 (1999) 3567.
[14] S.R. Manalis, S.C. Minne, C.F. Quate, Appl. Phys. Lett. 70 (1997) 3311.
[15] P.I. Oden, E.A. Wachter, P.G. Datskos, T. Thundat, R.J. Warmack, SPIE—Infrared Technol. XXII 2744 (1996) 345.
[16] P.I. Oden, P.G. Datskos, T. Thundat, R.J. Warmack, Appl. Phys. Lett. 69 (1996) 3277.
[17] J.K. Gimzewski, C. Gerber, E. Meyer, R.R. Schlittler, in: D.A.H.-J. Güntherodt, E. Mayer (Eds.), Forces in Scanning Probe Methods, Vol. 286, Kluwer Academic Publisher, Dordrecht, 1995, p. 123.
[18] M. Allegrini, C. Astoli, P. Baschieri, F. Dinnneli, C. Frediani, A. Lio, T. Mariani, Ultramicroscopy 42–44 (1992) 371.
[19] D. Sarid, Scanning Force Microscopy, Oxford University Press, New York, 1991.
[20] F. Ohnesorge, G. Binning, Science 260 (1993) 1451.
[21] J.H. Hoh, J.P. Cleveland, J.-P. Prater, P.K. Hansma, J. Am. Chem. Soc. 114 (1992) 4917.
[22] R.J. Young, Vacuum 44 (1993) 353.
[23] M.J. Vasile, C. Biddick, S. Schwalm, J. Vac. Sci. Technol. B12 (1994) 2388.
[24] S. Rajic, P.G. Datskos, I. Datskou, T.A. Marlar, in: A.C. Dubey, J.F. Harvey, J.T. Broach, R.E. Dugan, Detection and Remediation Technologies for Mines and Minelike Targets IV, Vol. 3710, SPIE, Bellingham, WA, 1999, p. 356.
[25] E.A. Wachter, T. Thundat, P.G. Datskos, P.I. Oden, S.L. Sharp, R.J. Warmack, Rev. Sci. Instrum. 67 (1996) 3434.
[26] R. Amantea, C.M. Knoedler, F.P. Pantuso, V.K. Patel, D.J. Sauer, J.R. Tower, SPIE, Vol. 3061, Orlando, FL, 1997, p. 210.
[27] P.G. Datskos, P.I. Oden, T. Thundat, E.A. Wachter, R.J. Warmack, S.R. Hunter, Appl. Phys. Lett. 69 (1996) 2986.